FOCUSING AND DIFFUSION PROCESSES IN MICROCHANNELS

Iulia Rodica DAMIAN[1], Steffen HARDT[2], Corneliu BĂLAN[3]

The paper investigates the hydrodynamic focusing phenomenon and post - focusing vortical structures within a cross shaped micro - junction with one main inlet, two lateral perpendicular branches and one outlet. The aim is to analyze the shape of the focused stream and vortical structures depending on the microchannel geometry, flow parameters and fluid properties. The flow is controlled by a pressure pump equipped with flow sensors. Qualitative images of the flow patterns are acquired using an inverted microscope. Numerical simulations performed by FLUENT code are found in good agreement with the experimental results.

Keywords: hydrodynamic focusing, vortical structures, microchannels, CFD, experimental investigations.

1. Introduction

In the fields of Lab-on-a-Chip devices, complex fluids rheometry, MEMS systems, molecular diagnosis, the hydrodynamic focusing phenomenon has various practical applications [1]. In microfluidics, these are related to flow control and transfer processes, such as positioning of cells and particles within a certain region of a microfluidic device, magnetic separation and sorting, particle filtration and extraction, micromixers, fabricating polymer microfibers having distinct shapes and material properties [2, 3, 4, 5, 6, 7], etc.

The present study investigates the hydrodynamic focusing phenomenon inside two cross junction microchannels. The aim was to comprehend and characterize the shape of the focused stream depending on the microchannel geometry, flow parameters and fluid properties. The flow visualization and the numerical modeling were focused on the evolution of the vortical structures in the region of cross linked branches of the junction. Numerical simulations performed by FLUENT code were found in good agreement with the experimental results.

[1] PhD Student, Reorom Group, Hydraulics Department, University POLITEHNICA of Bucharest, Romania, rodi.damian@upb.ro
[2] Prof. PhD. rer. nat., Nano- and Microfluidics Institute, Center of Smart Interfaces, Technische Universität Darmstadt, Germany
[3] Prof. PhD., Reorom Group, Hydraulics Department, University POLITEHNICA of Bucharest, Romania

2. Experimental procedure

The visualizations are performed in the median plane of a cross shaped microgeometry. In order to manufacture the transparent microchannels, we used the PDMS casting method and covered them with glass. The positive mold is obtained through soft litography, by SU8 deposition on a silicon wafer substrate. In order to obtain the PDMS solution, the base of the silicone elastomer is mixed with the curing agent in a 10:1 ratio. After degassing with a vacuum pump, the PDMS solution is poured over the mold. Heating of the substrate at 75 - 80^{o}C for 30 minutes leads to the solidification of the 3 mm silicone layer. After peeling off the PDMS layer we cut and separate the chips and ensure the access at the inlets and outlet of the microchannel for the fluidic nanoports. For the bonding process we placed the PDMS chip and the glass slide in a plasma chamber in presence of O_2. We bond the PDMS part and the glass substrate by putting them in contact and applying a slight pressure.

The cross section of the PDMS microchannels under consideration is rectangular; two aspect ratios (G_I - 100x100 μm and G_{II} - 200x100 μm) are investigated.

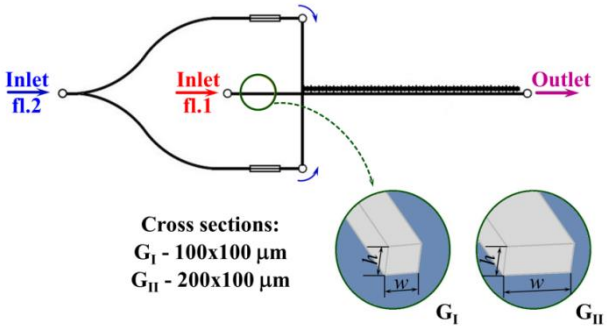

Fig. 1. A sketch of the flow configuration and geometry.

The pulseless flow is controlled using an ElveFlow pressure pump, equipped with flow rate sensors for the two inlets (main and secondary). In the lateral branches the flow is actuated by one single input (See Fig. 1). On the main path it is maintained constant and distinctive sample stream evolutions are investigated by varying the pressure on the lateral channels. For specific ratios of the inlets pressure, vortical structures are observed. The visualizations are performed using a Nikon Eclipse Ti microscope and the flow dynamics is recorded with an Andor iXonEM+ camera, while the image processing is done using the NIS Elements AR software.

Table 1

Investigated cases

Case	Fluids	
	i_1 - main inlet	i_2 - lateral branches
A	Dyed water	water
B	IPA	water

Water and Isopropanol alcohol are used for the sample stream, while for the lateral sheath streams only one working fluid is considered, as seen in Table 1 which summarizes the investigated cases (Case A and B). The properties of the fluids are presented in Table 2. For visualization purpose, in Case A, where the working fluid is the same, water, for both inlets, a dye (RITC - Rhodamine Isothiocyanate) is chosen to color the main stream. The appropriate illumination source is a Melles Griot Laser with a $\lambda_{ex} = 543$ nm excitation wavelength.

Table 2

Material characteristics of the fluids

Fluid	Density ρ [kg/m^3]	Viscosity η [Pas]
IPA	786	0.0025
water	1000	0.001

The dimensionless parameter that characterizes the flow is the Reynolds number:

$$Re = \frac{\rho V 4 R_h}{\eta} \tag{1}$$

where V is the average velocity at the inlet of the microchannel, R_h is the hydraulic radius, the characteristic length of the flow, ρ is the fluid density and η is the viscosity.

$$R_h = \frac{A}{P} \tag{2}$$

where A is the area of the inlet and P is the wetted perimeter.

$$A = hw, P = 2h + 2w \tag{3}$$

where h is the height and w is the width of the microchannel.

Because the secondary inlet separates in two lateral symmetrical branches perpendicular to the main channel, we can assume that $Re_{21} = Re_{22} = \frac{Re_2}{2}$.

For all the experiments, the input parameter at the main inlet is maintained constant ($p_1 = 200$ mbar), while for the secondary inlet, p_2 is increasing with a step of 1 mbar. P_2 is in the range of 520 - 531 mbar for G_I Case A and 521 – 536 for Case B. For G_{II}, p_2 is increased in the range 744 – 767 mbar and 722 – 734

mbar for Case A and Case B respectively. At the outlet of the chip p_0 is the atmospheric pressure. Because the pressure pump is equipped with flow rate sensors, for each moment of time the data of pressure and flow rate are acquired.

3. Experimental results

Using the setup based on the microscope equipped with the camera, microfluidic pump and chip, direct visualization and qualitative and quantitative observations of the flow dynamics are obtained.

In the present study experimental and numerical results regarding the formation and evolution of post focusing vertical structures are presented.

As the flow velocity increases on the two lateral branches, the location at which a thread is destabilized is observed to move toward the micro - junction as seen in Fig. 2 and Fig. 3. This observation is valid for both the analyzed cases and considered geometries (G_I and G_{II}), where the focused stream is the same as the sheath streams (Case A), or different (case B).

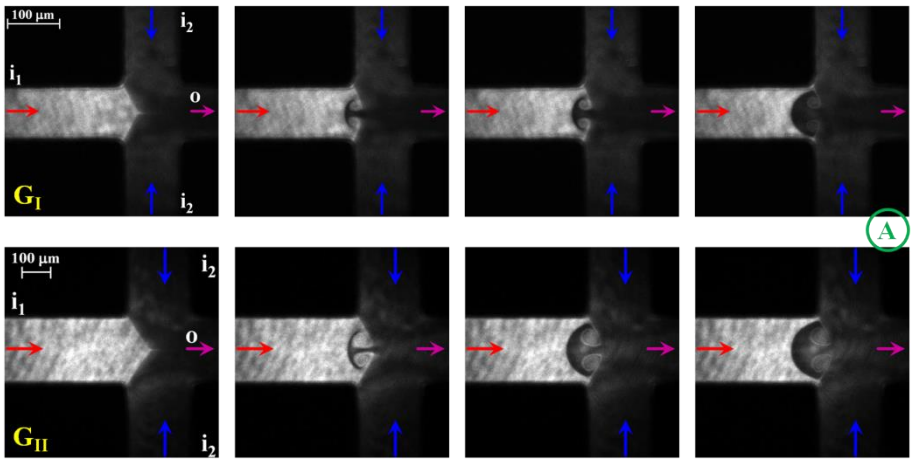

Fig. 2. Visualizations of the flow focusing and the formation of the post-focusing vortical structures for the investigated microgeometries (G_I - 100x100 µm, G_{II} - 200x100 µm), in case A: i_1 - dyed water, i_2 - water.

The shape of the vortical structures is different for the two geometries, thus offering information on the Aspect Ratio $\left(AR = \frac{w}{h}\right)$ influence on the flow dynamics (Fig. 2).

Experimentally it is noticed that the main stream is more and more focused with the increase of the input parameters on the secondary inlet. Because the two sheath streams are symmetrically positioned at a 90^o angle relatively to the main channel, the focused jet and the vortexes are identical relatively to the symmetry plane of the micorchannel.

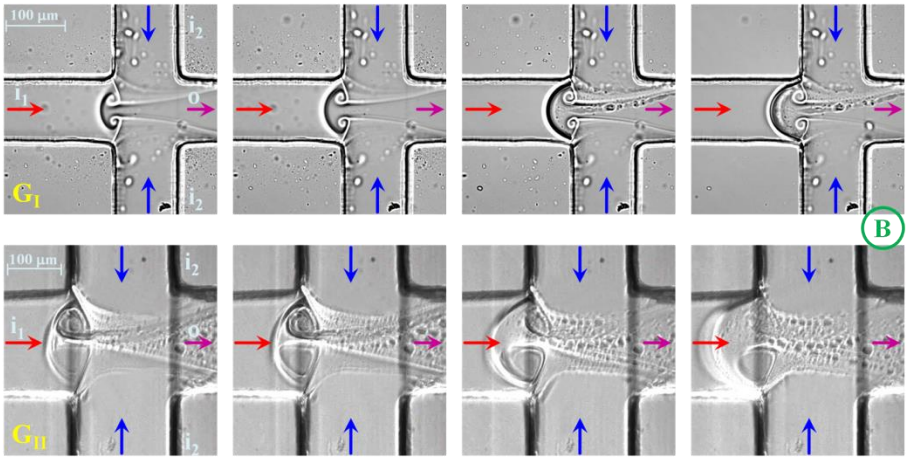

Fig. 3. Visualizations of the post-focusing vortical structures for the investigated microgeometries (G_I - 100x100 µm, G_{II} - 200x100 µm), in case B: i_1 - IPA, i_2 - water.

In Fig. 2 are presented the experimental results for Case A, where the same fluid is used for both the inlets of the micro - junction. The Aspect Ratios are 1 and 2 respectively for the two geometries.

When Isopropyl alcohol is flowing through the main channel (Fig. 3), from the direct visualizations are highlighted the vortices that have similar structures as those in Case A, for the respective Aspect Ratios.

The influence of the chosen fluids is not as relevant on the shape of the vortex, as the influence that the Aspect Ratio of the microchannel has.

4. Numerical simulations

The numerical results presented in this paper are based on the solution of the Navier - Stokes equation for an incompressible Newtonian fluid flow inside the microchannel and on the continuity equation:

$$\rho\left(\frac{\partial \boldsymbol{v}}{\partial t} + (\boldsymbol{v}\cdot\boldsymbol{\nabla})\boldsymbol{v}\right) = -\boldsymbol{\nabla}p + \eta\Delta\boldsymbol{v}$$

$$\boldsymbol{\nabla}\cdot\boldsymbol{v} = 0 \tag{4}$$

where v is the velocity vector, ρ and η are the density and viscosity, respectively and p represents the pressure.

These are coupled with the diffusion equation for a concentration field:

$$\frac{\partial c}{\partial t} + (\boldsymbol{v}\cdot\boldsymbol{\nabla})c = D\Delta c \tag{5}$$

where c is the concentration and D is the diffusion coefficient [4].

The diffusion coefficients of the working fluids are indicated in Table 3 and were set as User Defined Scalars (UDS) [8].

The numerical approach of the study is based on the configuration of the microchannels used in the experimental procedure. Due to the symmetry of the flow, a symmetrical 3D flow domain was generated using the pre - processor Gambit. All numerical simulations were performed using Ansys - FLUENT code. The 3D mesh contains 1.137.500 hexahedral cells for G_I and 1.343.750 for G_{II}.

Table 3

Diffusion coefficients of the fluids

Fluid	Diffusion coefficient $\mathbf{D}\cdot 10^{-10}$ [m^2/s]
IPA	$\mathbf{D_{IPA\text{-}w}} = 6.13$
water	$\mathbf{D_{w\text{-}IPA}} = 9.66$

In order to perform the CFD analysis, the proper boundary conditions are imposed. These are shown in Fig. 4 along with a schematic of the flow domain and mesh details. For Case B, the equations (4) and (5) are coupled with the Volume of Fluid (VOF) model available in FLUENT [8]. For numerical simulations corresponding to the experiments in Case A, the viscous laminar model was used. All solutions are obtained with the unsteady solver.

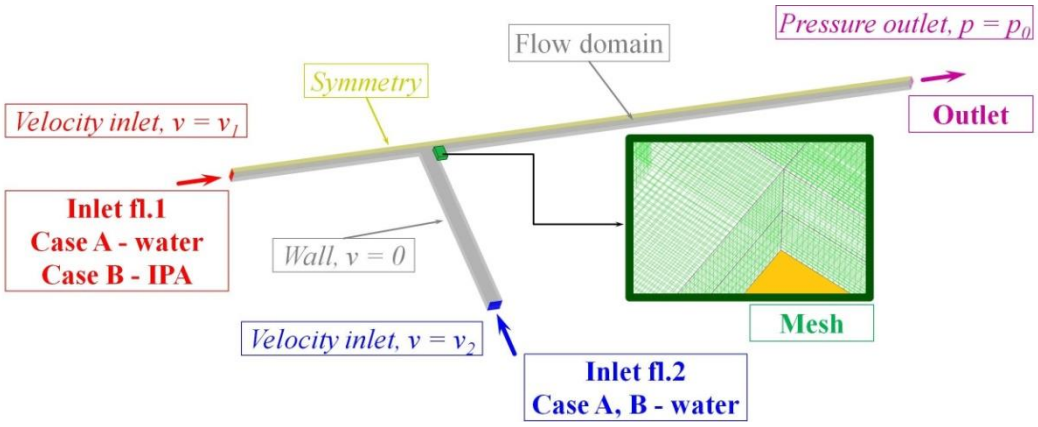

Fig. 4. Detail on the numerical flow domain discretization and the boundary conditions implemented in FLUENT code for the two cases A (i_1 - dyed water, i_2 - water) and B (i_1 - IPA, i_2 - water).

The good correlation between the experimental visualizations and the predicted pathlines by the 3D numerical simulations is obvious for all cases. The vortex diameter is enlarged with the increase of input parameter for i_2 (Fig. 5).

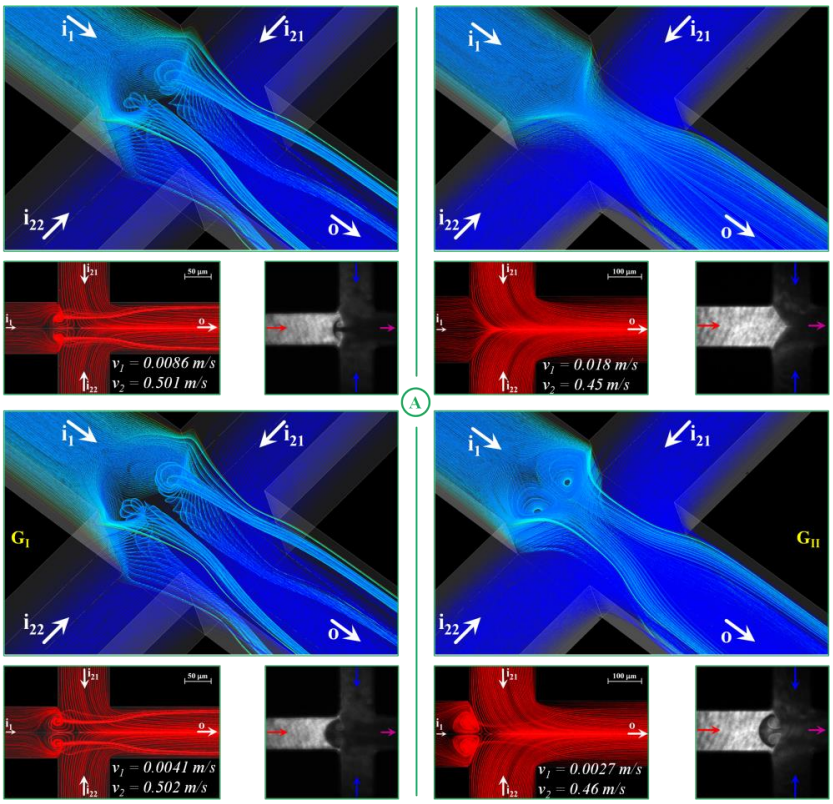

Fig. 5. Numerical flow patterns in case A: right - G_I - vortical structures, left - G_{II} - hydrodynamic focusing and vortical structure.

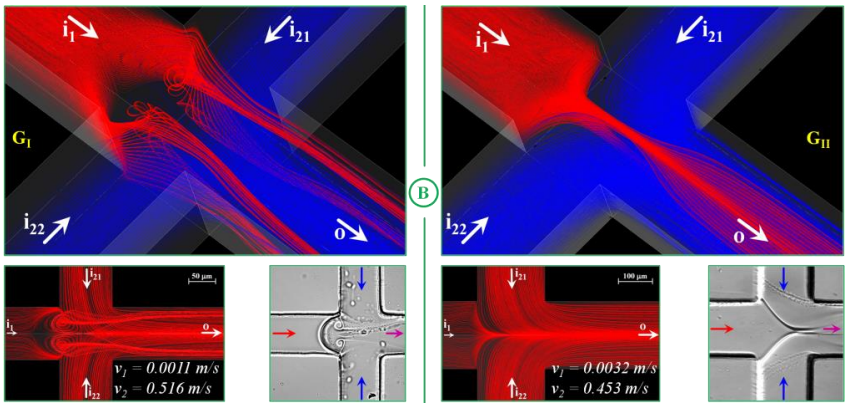

Fig. 6. Numerical flow patterns in case B: right - G_I - hydrodynamic focusing, left - G_{II} - vortical structure.

In Fig.5 and 6 are shown the 3D views of the numerical results representing the flow of different fluids inside the two microchannels, along with a comparison of the view in median plane with the experimental visualizations.

5. Conclusion and final remarks

An experimental and numerical study on the flow inside cross – microjunctions was presented. The objective of the paper was to examine the influence of the microchannel aspect ratio and of the fluid properties upon the vortex formation and its characteristics. It is a starting point for investigation of the diffusion process between different fluids. The results reveal a good qualitative correspondence between simulation and experiment.

Acknowledgement

Iulia Rodica Damian's work has been funded by the Sectoral Operational Programme Human Resources Development 2007-2013 of the Ministry of European Funds through the Financial Agreement POSDRU/159/1.5/S/132397. The authors acknowledge the financial support from the grant of the Ministry of National Education, CNCS – UEFISCDI, project number PN-II-ID-PCE-2012-4-0245. The authors acknowledge the technical support of the group form Nano- and Microfluidics Institute, Center of Smart Interfaces, TU Darmstadt, Germany.

R E F E R E N C E S

[1] *W. Zhigang, N. Nam Trung*, "Hydrodynamic focusing in microchannels under consideration of diffusive dispersion: Theories and experiments", in Sensors and Actuators, B: Chemical, **vol. 107**, 2005, pp. 965 - 974.

[2] *J. P. Golden, G. A. Justin, M. Nasir, F. S. Ligler*, "Hydrodynamic focusing-a versatile tool", in Analytical and Bioanalytical Chemistry, **vol. 402**, 2012, pp. 325 - 335.

[3] *M. Hoffmann, M. Schlüter, N. Räbiger*, "Experimental investigation of liquid-liquid mixing in T-shaped micro-mixers using μ-LIF and μ-PIV", in Chemical Engineering Science, **vol. 61**, 2006, pp. 2968 - 2976.

[4] *S. H. Wong, M. C. L. Ward, C. W. Wharton*, "Micro T-mixer as a rapid mixing micromixer", in Sensors and Actuators, B: Chemical, **vol. 100**, 2004, pp. 359 - 379.

[5] *F. J. Galindo-Rosales, M. A. Alves, M. S. N. Oliveira*, "Microdevices for extensional rheometry of low viscosity elastic liquids: a review", in Microfluidics and Nanofluidics, **vol. 14**, Iss. 1-2, 2012, pp. 1 - 19.

[6] *A. Lanzaro, Z. Li, X. F. Yuan*, "Quantitative characterization of high molecular weight polymer solutions in microfluidic hyperbolic contraction flow", in Microfluidics and Nanofluidics, **vol. 18**, 2015, pp. 819-828.

[7] *Y. N. Wu, T. T. Fu, Y. G. Ma, H. Z. Li*, "Active control of ferrofluid droplet breakup dynamics in a microfluidic T-junction", Microfluidics and Nanofluidics, **vol. 18**, Iss. 1, pp. 19 - 27.

[8] ***Fluent Inc., Fluent 6.3 User's Manual, 2008.